

We are IntechOpen, the world's leading publisher of Open Access books Built by scientists, for scientists

6,900

Open access books available

185,000

International authors and editors

200M

Downloads

Our authors are among the

154

Countries delivered to

TOP 1%

most cited scientists

12.2%

Contributors from top 500 universities



WEB OF SCIENCE™

Selection of our books indexed in the Book Citation Index
in Web of Science™ Core Collection (BKCI)

Interested in publishing with us?
Contact book.department@intechopen.com

Numbers displayed above are based on latest data collected.
For more information visit www.intechopen.com



Phononic Crystals and Thermal Effects

Arafa H. Aly and Ahmed Mehaney

Abstract

In this work, we demonstrate a comprehensive theoretical study of one-dimensional perfect and defect phononic crystals. In our study, we investigate the elastic and shear waves with the influences of thermal effects. The numerical calculations based on the transfer matrix method (TMM) and Bloch theory are presented, where the TMM is obtained by applying the continuity conditions between two consecutive sub-cells. Also, we show that by introducing a defect layer in the perfect periodic structures (defect phononic crystals), we obtain localization modes within the band structure. These localized modes can be implemented in many applications such as impedance matching, collimation, and focusing in acoustic imaging applications. Then, we investigate the influences of the incident angle and material types on the number and intensity of the localized modes in both cases of perfect/defect crystals. In addition, we have observed that the temperature has a great effect on the wave localization phenomena in phononic band gap structures. Such effects can change the thermal properties of the PnCs structure such as thermal conductivity, and it can also control the thermal emission, which is contributed by phonons in many engineering structures.

Keywords: thermal emission, dispersion relation, phononic band gap, localized modes

1. Introduction

Phononic crystals (PnCs) are new composite materials which can interact, manipulate, trap, prohibit, and transmit the propagation of mechanical waves. Recently, great efforts have been dedicated to study these novel materials to be used in many potential engineering applications. By reference to the meaning of idiom, the term “phononic” was derived in analogy to the term “phonon,” which is considered as a quantization of the lattice vibrations. In the previous conscious of science, these vibrations are impossible to be controlled because the atoms in the solid cannot move independently of each other because they are connected by chemical bonds. By appearing PnCs, this assumption was changed and the mechanical wave can be filtered, transmitted, stopped, and localized within specific frequencies called phononic band gaps [1, 2].

Within the phononic band gaps, the mechanical waves of all types are greatly blocked. Actually, the formation of the phononic band gaps is back to the variation in the mechanical properties of the materials that build the PnC structure. Therefore, Bragg interference at the interface between each two materials can be

obtained. As a result, the phononic band gaps and transmission bands are formed. Moreover, novel properties such as negative refraction and acoustic metamaterials are presented in PnC structures [3–7]. These novel properties of PnCs can be utilized in many industrial and engineering applications such as MEMS applications, filters, waveguides, clocking, multiplexers, and sensor applications [8–12].

As it is well-known, the physical origin of all crystal structures has the same idea of the design. Photonic crystals and semiconductor devices could not develop such types of the previous applications. From the scientific point of view, we should mention that the physical nature of PnCs is different from one of photonic crystals, as well as semiconductors. Generally, the various forms of waves are referred to as: electron waves as scalar waves and optical waves as vector waves, while elastic waves as tensor waves [13–19].

As a result, to design PnCs having a complete phononic band gap, the mechanical properties must be changed not only in one direction (i.e. x -direction) but also in all three directions of space (i.e., x , y , and z directions). Therefore, PnCs can be classified according to the periodicity into three types, i.e., the one-dimensional (1D), the two-dimensional (2D), and the three-dimensional (3D) PnCs [20–24]. PnCs can control the entire spectrum of phonons frequency from 1 Hz to THz range. As it is well-known, the waves that propagate through solid media are called elastic waves, while those that propagate through fluids are called acoustic waves. Also, PnCs can control the different types of mechanical waves such as elastic waves, acoustic waves, and surface waves. Therefore, unlike photonic crystals, not all 3D PnCs possess complete phononic band gaps. PnCs must possess band gaps for both elastic and acoustic waves at the same frequency region. Consequently, we have to fabricate PnC structures for both solid and fluid media [25–28]. Hence after, these different polarizations introduce more challenges to PnCs higher than other crystal, which in turn makes the theoretical manipulation of PnCs more attractive and perspective.

From the previous observations of PnCs structures, several methods were developed to calculate the phononic band gaps such as Plane-Wave-expansion Method (PWM), Bloch-Floquet Method (BFM), and finite difference time-domain method (FDTD) [29–33]. In this chapter, we will depend on the Transfer Matrix Method (TMM) [34] for calculating the reflection coefficient and the transmission coefficient of the one-dimensional PnC structure. Such method considered very suitably for the 1D structure due to its recursive nature, since it allows the continuity of the waveform at the interface between each two layers [35, 36]. Also, by using the TMM, we can obtain the dispersion relations of the mechanical waves through the periodic PnC structures. PnCs and temperature are in mutual influences in several ways [37]. For example, at any temperature, mainly the huge contribution in the thermal conductivity of many materials is dominant by phonon contribution, which is a function of phonon mean free path and the Boltzmann distribution of phonons of any material. Also, the thermal conductivity is depending on the thickness of a material, where optical branches contribute with about 30% of the thermal conductivity of any material. By inhibiting the acoustic phonon population, the optical phonon relaxation is indirectly inhibited by up to 30% and hence limits their contribution to thermal conductivity. Furthermore, in silicon PnC, the thermal contribution of phonons has been reduced to less than 4% of the value for bulk silicon at room temperature [38–40].

Moreover, the defected PnCs structures have wonderful application in wave guiding and multiplexing. But the produced structures are different from the proposed ideal structures due to the errors and defaults in manufacturing. By removing some layers or materials from the ordered periodic structure in a PnC, we can create a point or a waveguide defects that are able to localize and bend signals. Such

mechanism has been implemented similarly in photonic crystals to slow light. Consequently, the produced waveguides in PnCs structures can be used in focusing and collimation of acoustic waves in medical ultrasound applications, sensors, and MEMS applications [2, 41–44].

In the present work, we introduce the formation of phononic band gaps under the influences of many physical parameters. First, the general case of SH-wave propagation in arbitrary direction will be investigated by using TMM with calculation of the dispersion curves as well. Also, the influences of the incident angle on the band gaps are analyzed and discussed. In addition, this work focuses on correlating and comparing the results of SH-waves with in-plane waves propagating normally to the structure. For the in-plane waves, the reflection coefficients for S- and P-waves are plotted and compared with the dispersion relations curves. Furthermore, we are demonstrating the wave localization phenomenon in PnCs and the effects of the temperature on the band structure of PnCs and the localized modes for both in-plane and SH-waves. Also, the numerical results are presented and discussed to investigate the effect of the defect layer on the wave localization modes inside the structures. Finally, the effects of the thickness and type of the defect layer material on the band gap structure had been discussed.

2. Theoretical analysis and numerical models

2.1 Equation of wave propagation

Figure 1 shows the schematic diagram of the 1D PnC crystal structure. The proposed crystal structure has an infinite number of the periodically arranged unit cells. The unit cell may include two or more layers; here, we propose that it is made by only two materials *A* and *B*, respectively. The two materials are labeled by the subscript $j = 1, 2$. Also, the thickness of the unit cell (the lattice constant) is $a = a_1 + a_2$. The thickness, Lamé' constant, shearing modulus, Poisson's ratios, mass density, and Young's modulus of the two layers are denoted by equation $a_j, \lambda_j, \mu_j, \nu_j, \rho_j, E_j$ [$E_j = \lambda_j(1 + \nu_j)(1 - 2\nu_j)/\nu_j$, respectively].

The governing equation of anti-plane shear waves (SH-waves) polarized in the z -direction propagated in the xy -plane can be written in the following form [45–47].

$$\mu_j \nabla^2 \varphi_j(x_j, y_j, t) + \sigma_j^{tx} \frac{\partial^2 \varphi_j^2(x_j, y_j, t)}{\partial x^2} = \rho_j \ddot{\varphi}_j(x_j, y_j, t) \quad (j = 1, 2), \quad (1)$$

where T is the temperature variation, β_j is the thermal expansion coefficients, $\varphi_j(x_j, y_j, t)$ is the displacement components along the z -direction, t is the time,

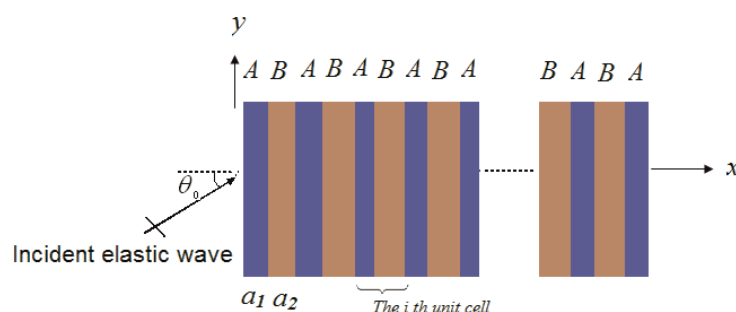


Figure 1.
 A schematic diagram of a perfect 1D binary PnC structure.

$\sigma_j^{tx} = -E_j \beta_j T / (1 - 2\nu_j)$ is the thermal stress, and $\nabla^2 = \partial/\partial x_j^2 + \partial/\partial y_j^2$ is the Laplacian operator. The solution $\phi_j(x_j, y_j, t)$ in the j th layer with time harmonic dependence can be expressed as [48],

$$\phi_j(x_j, y_j, t) = \phi_j(x_j) \exp \left[iky_j \sin \theta_0 - i\omega t \right], \quad (2)$$

Where, c is the velocity component of the incident wave, $i^2 = -1$, $k = \omega/c$ is the wave number, θ_0 is the angle of the incident wave, ω is the angular frequency, and ϕ_j is the amplitude.

In many cases, it is more convenient to represent the thickness value by the following dimensionless coordinates:

$$\xi_j = x_j/\bar{a}_1, \eta_j = y_j/\bar{a}_1 \quad (j = 1, 2), \quad (3)$$

where \bar{a}_1 is the average thickness value of the material A . \bar{a}_1 is equal to a_1 for the periodic structures. By inserting Eq. (3) in Eqs. (1) and (2), we can obtain the following wave equations:

$$\phi_j(\xi_j, \eta_j, t) = \phi_j(\xi_j) \exp \left[i\alpha\eta_j \sin \theta_0 - i\omega t \right], \quad (4)$$

$$\left(1 + \chi_j \right) \frac{d^2 \phi_j}{d\xi_j^2} - \alpha^2 \left(\sin^2 \theta_0 - \frac{\alpha_j^2}{\alpha^2} \right) \phi_j = 0, \quad (5)$$

where c_j represents the wave velocity in each material, $\chi_j = \sigma_j^{tx}/\mu_j$ is the stress and shearing modulus ratio, $\alpha = k\bar{a}_1$ represents the SH-waves dimensionless wave number, $\alpha_j = k_j\bar{a}_1$ is the dimensionless wave number and $k_j = \omega/c_j$ is the wave vector of materials A and B , respectively. Eq. (5) has a general dimensionless solution, and it is given in the following form,

$$\phi_j(\xi_j) = A_j \exp \left(-i\alpha q_j \xi_j \right) + B_j \exp \left(+i\alpha q_j \xi_j \right), \quad (j = 1, 2), \quad (6)$$

where A_j and B_j are unknown coefficient to be determined, and q_j is a parameter and has the value $q_j = \frac{1}{\sqrt{1+\chi_j}} \sqrt{c^2/c_j^2 - \sin^2 \theta_0}$. Therefore, the dimensionless solution $\phi_j(\xi_j, \eta_j, t)$ with time harmonic dependence is:

$$\phi_j(\xi_j, \eta_j, t) = \left(A_j \exp \left(-i\alpha q_j \xi_j \right) + B_j \exp \left(+i\alpha q_j \xi_j \right) \right) \left(\exp \left[i\alpha\eta_j \sin \theta_0 - i\omega t \right] \right). \quad (7)$$

2.2 Transfer matrix method

The dimensionless shear stress component is given as follows:

$$\tau_{xzj} = \mu_j \frac{\partial \phi_j}{\partial \xi_j} \quad (j = 1, 2). \quad (8)$$

Assuming that the PnC consists of n unit cells, the boundary conditions at the left and right sides of the two layers in the i th unit cell can be written in the following form [45],

$$\begin{aligned}\phi_{jL}^{(i)} &= \phi_j^{(i)}(0), \quad \phi_{jR}^{(i)} = \phi_j^{(i)}(\xi_j), \\ \tau_{xjL}^{(i)} &= \mu_j^{(i)} \frac{\partial \phi_j^{(i)}}{\partial \xi_j}(0), \quad \tau_{xjR}^{(i)} = \mu_j^{(i)} \frac{\partial \phi_j^{(i)}}{\partial \xi_j}(\xi_j) \quad (i = 1, 2, \dots, n),\end{aligned}\quad (9)$$

where the subscripts L and R denote the left and right sides of the two layers, and $0 \leq \xi_j \leq \zeta_j = a_j/\bar{a}_1$ ($j = 1, 2$) are the dimensionless thicknesses of materials A and B . Substituting Eqs. (7) and (8) into Eq. (9), the following matrix equation can be obtained as follows:

$$\nu_{jR}^{(i)} = T'_j \nu_{jL}^{(i)} \quad (j = 1, 2; i = 1, 2, \dots, n), \quad (10)$$

where $\nu_{jR}^{(i)} = \left\{ \phi_{jR}^{(i)}, \bar{a}_1 \tau_{xjR}^{(i)} \right\}^T$ and $\nu_{jL}^{(i)} = \left\{ \phi_{jL}^{(i)}, \bar{a}_1 \tau_{xjL}^{(i)} \right\}^T$ are the dimensionless state wave vectors at right and left sides of each unit cell and T'_j is the 2×2 transfer matrix of each unit cell. The four elements of T'_j can be written in the following forms,

$$\begin{aligned}T'_{j(1,1)} &= \frac{\exp(i\alpha q_j \zeta_j) + \exp(-i\alpha q_j \zeta_j)}{2}, \quad T'_{j(1,2)} = \frac{\exp(i\alpha q_j \zeta_j) - \exp(-i\alpha q_j \zeta_j)}{2i\alpha q_j \mu_j}, \\ T'_{j(2,1)} &= \frac{i\alpha q_j \mu_j \left[\exp(i\alpha q_j \zeta_j) - \exp(-i\alpha q_j \zeta_j) \right]}{2}, \quad T'_{j(2,2)} = T'_{j(1,1)}.\end{aligned}\quad (11)$$

2.3 Characteristic of the dispersion relation

At the interface between the layers, the following condition is satisfied:

$$\nu_{1R}^{(i)} = \nu_{2L}^{(i)}. \quad (12)$$

Thus, the relationship between the right and left sides of the i th unit cell can be obtained from Eq. (10) as follows:

$$\nu_{2R}^{(i)} = T_i \nu_{1L}^{(i)} \quad (i = 1, 2, \dots, n), \quad (13)$$

where T_i is the accumulative transfer matrix of the i th unit cell and can be written in the following form:

$$T_i = T'_2 T'_1. \quad (14)$$

At the interface between the right side of the unit cell and the left side of the i th unit cell, the following condition is satisfied:

$$\nu_{1L}^{(i)} = \nu_{2R}^{(i-1)} \quad (i = 2, \dots, n). \quad (15)$$

By equating Eqs. (13) and (15), we can obtain the relationship between the state vectors of the $(i - 1)$ th unit cells and the i th unit cell in the following form:

$$\nu_{2R}^{(i)} = T_i \nu_{2R}^{(i-1)} \quad (i = 2, \dots, n), \quad (16)$$

Therefore, T_i represents the transfer matrix between each two successive unit cells.

By using Floquet and Bloch theories, we can obtain the displacement and stress fields between each two neighboring unit cells (at the interface) by the following relations [46–49]:

$$\phi_{2R}^{(i)} = \phi_{2R}^{(i-1)} \exp(ika), \quad \tau_{xz2R}^{(i)} = \tau_{xz2R}^{(i-1)} \exp(ika), \quad (17)$$

where k is the wave number representing the direction of the traveled wave across the structure. Combining the above two equations leads to the following matrix equation:

$$\nu_{2R}^{(i)} = \nu_{2R}^{(i-1)} \exp(ika) \quad (i = 2, \dots, n). \quad (18)$$

By equating Eqs. (16) and (18) which leads to the following eigenvalue problem:

$$|T_i - e^{ika} I| = 0. \quad (19)$$

Eq. (19) can be rewritten as follows:

$$T_i \nu_{2R}^{(i-1)} = \lambda \nu_{2R}^{(i-1)}, \quad (20)$$

where $\lambda = e^{ika}$ is a complex eigenvalue and $\nu_{2R}^{(i-1)}$ is a complex eigenvector.

2.4 Band structure formation

The wave number in Eqs. (17) and (18) is a complex number, so it can be a positive or negative number; in general, the wave number can be written in the following form [50]:

$$k = k_{\text{real}} - ik_{\text{imaginary}}, \quad (21)$$

where k_{real} and $k_{\text{imaginary}}$ are the real and imaginary wave numbers, respectively. Therefore, we can deduce from this relation that the complex wave number has two forms, so it can inhibit the incident waves within the phononic band gaps. Consequently, we have two frequency ranges and they are organized as follows:

1. If $k = k_{\text{real}}$ and $k_{\text{real}} > 0$.

From Eq. (18),

$$\begin{aligned} \nu_{2R}^{(i)} &= \nu_{2R}^{(i-1)} e^{ika}, \\ \nu_{2R}^{(i)} &= \nu_{2R}^{(i-1)} e^{i|k_{\text{real}}|a}. \end{aligned} \quad (22)$$

From Eq. (22), we can deduce that the displacement and stress at the successive unit cells (i) th and $(i - 1)$ th are differ only by a phase factor $e^{i|k_{\text{real}}|a}$. At this condition, the elastic waves are allowed to propagate freely through the PnC structure with the corresponding frequencies and wave number, forming the so-called transmission bands.

2. If $k = -ik_{\text{imaginary}}$ and $k_{\text{imaginary}} < 0$

From Eq. (18),

$$\begin{aligned} v_{2R}^{(i)} &= v_{2R}^{(i-1)} e^{ika}, \\ v_{2R}^{(i)} &= v_{2R}^{(i-1)} e^{-|k_{\text{imaginary}}|a}. \end{aligned} \quad (23)$$

In contrast to the above case, we can deduce from Eq. (23) that the displacement and stress at successive unit cells (i)th and ($i - 1$)th are the same and do not have a phase difference. Moreover, the incident wave has an exponential spatial attenuation of strength magnitude proportional to the value $|k_{\text{imaginary}}|$. Hence after, at this case, the waves are prohibited from propagation in the PnC structure, which in turn, results in formation of the so-called phononic band gaps or stop bands.

2.5 Temperature influences on PnCs

When a mechanical wave propagates through a PnC structure, resultant vibrations occur which may increase or decrease phonons motions. Therefore, it can heat or cool the PnC structure. Also, the thermal expansion of the constituents materials may change, which will affect the mechanical constants of the material as well. Since the vibrations occur very rapidly, there is no big chance to thermal energies to flow and the elastic constants measured by elastic waves propagation are changed adiabatically. The elastic constants are connected to the isothermal constants by the following relation [51–55],

$$\lambda^\sigma = \lambda^\theta + \frac{9\beta^2 B^2 \theta}{\rho C_\nu}, \quad \mu^\sigma = \mu^\theta, \quad (24)$$

where the superscripts σ and θ indicate adiabatic and isothermal constants, β is the thermal expansion coefficient, B is the bulk modulus ($B = \lambda + 2/3\mu$), C_ν is the specific heat at constant volume, θ is the absolute temperature, and ρ is the mass density. From Eq. 24, we can deduce that λ^σ and λ^θ are not the same and the difference between them should be considered.

In addition to the above relations, if the temperature is increased, not only the wave velocities will increase but also the thickness of each layer will change by the following relation [53]:

$$\Delta a = \beta a_i \Delta t, \quad (25)$$

where Δa is the thickness difference of any layer, a_i is the original layer thickness, and Δt is the temperature difference. Hence after, these two variables will affect the longitudinal waves speed and the stress component in SH-waves equations. Since the P-wave velocity is $c_P = \sqrt{\frac{\lambda+2\mu}{\rho}}$, which, in turn leads to the variation of the band structure and band gaps properties.

3. Numerical examples and discussions

3.1 SH-waves results

First, from a practical point of view, the number of layers in the 1D PnC structure should take a finite number. Therefore, we consider the unit cell of the PnC structure is made from two layers. The two layers are lead and epoxy materials

and denoted by the symbols A and B , respectively. Second, dispersion relations are plotted for an infinite number of unit cells because it depends on Bloch theory that manipulates the propagation of waves through infinite periodic structures. Therefore, the dispersive behavior of the periodic materials and structures with an arbitrary chosen unit cell configuration is considered as an example. The constants of the materials used in the calculations can be found in Refs. [46, 49] and in **Table 1**. Here, we consider the velocity c of the incident wave is 800 m/s and the angle of the incidence is $\theta_0 = 20^\circ$. Also, the ambient temperature is proposed to be $T = 20^\circ\text{C}$. The dispersive properties of the inhomogeneous structures are determined by the properties ratios of the constituent materials, here we consider the two materials thicknesses ratio as 1:1.

Figure 2 presents the dispersion relation of SH-waves in the first Brillouin zone, and it is plotted between the nondimensional frequency $q = \omega a/c_B$ and the nondimensional wave number $\xi = k \times a$, where c_B is the wave velocity in the second material (epoxy). We considered the range of the nondimensional frequency is $0 \leq q \leq 9$. From this figure, we can conclude that, first, there are some

Materials	Mass density $\rho \times 10^3$ (kg/ m ³)	Lame' constant $\lambda \times 10^{10}$ (N/m ²)	Shearing modulus $\mu \times 10^{10}$ (N/m ²)	Young's modulus $E \times 10^{10}$ (N/m ²)	Poisson's ratios ν	Thermal expansion coefficient $\beta \times 10^{-6}$ (1/°C)	Specific heat $C_v \times 10^3$ (J/kg. °C)
Lead	11.4	3.3	0.54	1.536	0.43	29.5	0.128
Epoxy	1.180	0.443	0.159	0.435	0.368	22.5	1.182
Aluminum	2.699	6.1	2.5	6.752	0.355	23.9	0.9
Gold	19.32	15.0	2.85	8.114	0.42	14.2	0.13
Nylon	1.11	0.511	0.122	0.357	0.4	50	1.70

Table 1.
Material constants.

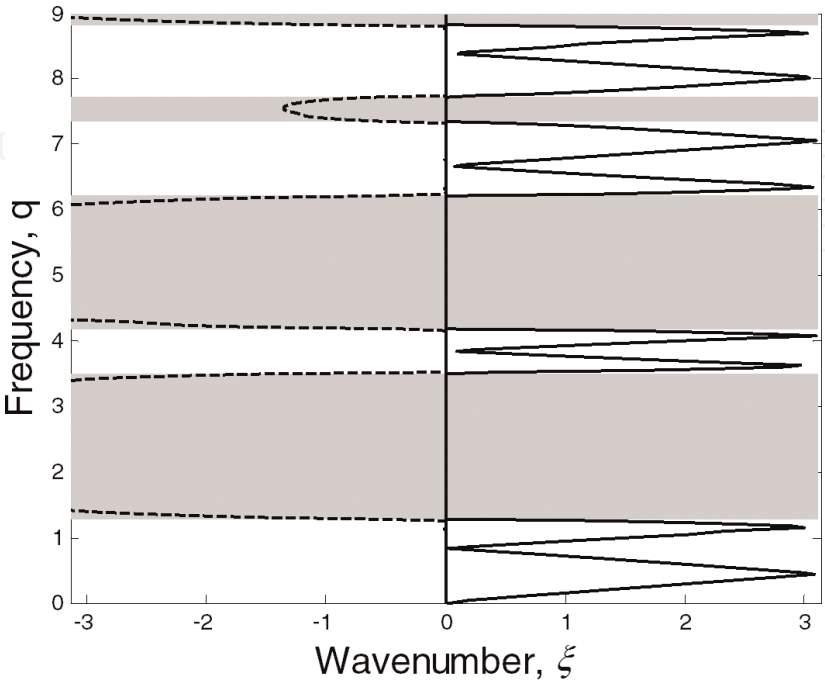


Figure 2.
The dispersion curve of SH-waves incident on the face of the 1D binary perfect PnC structure. Each unit cell consists of lead and epoxy materials (stop-bands shaded by the gray color).

frequency regions that are plotted with the white color and represent the real valued wave number and pass bands. Second, the other frequency regions corresponding to the imaginary wave number represent the phononic band gaps.

3.1.1 Influence of the angle of incidence on the phononic band gap

Figure 3(a) and **(b)** show the effects of the incident angle θ_0 on the band structures of the previous perfect structure. It can be seen that the wave propagation behavior of the perfect PnC changes obviously for different incident angles. For example, the stop bands for $\theta_0 = 15^\circ$ become a pass band for $\theta_0 = 45^\circ$. With increasing value of the incident angle, the same stop bands became wider in the considered frequency regions. However, in **Figure 3(c)**, we can note a wonderful phenomenon appeared when the angle θ_0 reached the value 85° . The stop band increased to be the entire band structure of the PnC, and no propagation bands were observed. The explanation of such phenomenon is deduced from the parameter

$q_j = \frac{1}{\sqrt{1+\chi_j}} \sqrt{c^2/c_j^2 - \sin^2\theta_0}$; if c/c_j become smaller than $\sin\theta_0$, the displacement field will decay. Therefore, a total reflection to the elastic waves will be occurred, where all the incident wave energy is reflected back to the structure and no waves are allowed to propagate through the PnC structure.

3.1.2 Defective mode effect on the band structure of the PnC

As shown in **Figure 4**, the dispersion relation of the perfect PnC structure will differ than the defected ones. We consider a defect layer from aluminum (the defect layer thickness $a_d = a_A$ i.e., 1/2 of any unit cell thickness) was immersed after the second unit cell, and the material properties are mentioned in **Table 1**. From **Figure 5**, it was indicated that elastic waves can be trapped within the phononic band gap and the band structure changed significantly than the perfect ones. The width of the band gaps increased due to the increment of mismatch between the constituent materials, this back to the insertion of a second interface inside the PnC structure. Moreover, the defect layer acts as a trap inside the PnC structure, so a special wave frequency corresponding to that waveguide will propagate through the structure.

Additionally, in **Figure 6(a)** ($a_d = 2a_A$) and **Figure 6(b)** ($a_d = 4a_A$), we studied the effects of the defect layer thickness on the position and number of the localized modes inside the band structure of the PnC. It was shown that the number and width of the localized modes were increased by increasing the defect layer thickness. Therefore, with increasing the thickness of the defect layer inside the periodic PnC structure, the localized modes within the band gap are strongly confined within the defect layer.

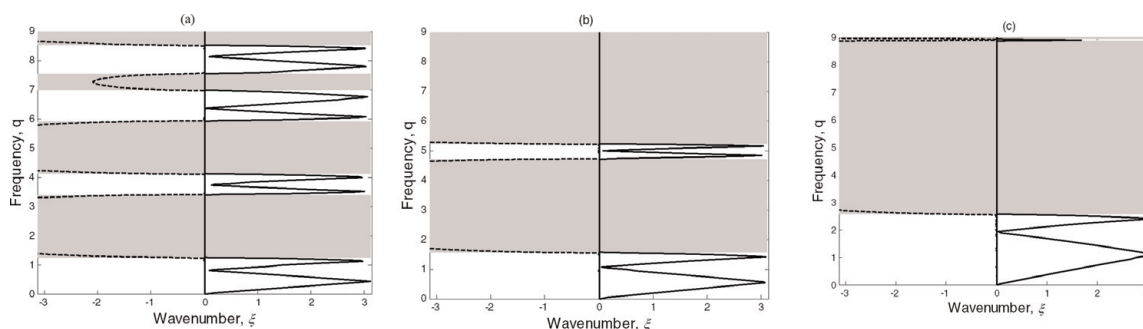


Figure 3.
 The calculated dispersion curves of SH-waves in a 1D binary perfect PnC at the incident angles (a) $\theta_0 = 30^\circ$, (b) $\theta_0 = 50^\circ$, and (c) $\theta_0 = 70^\circ$.

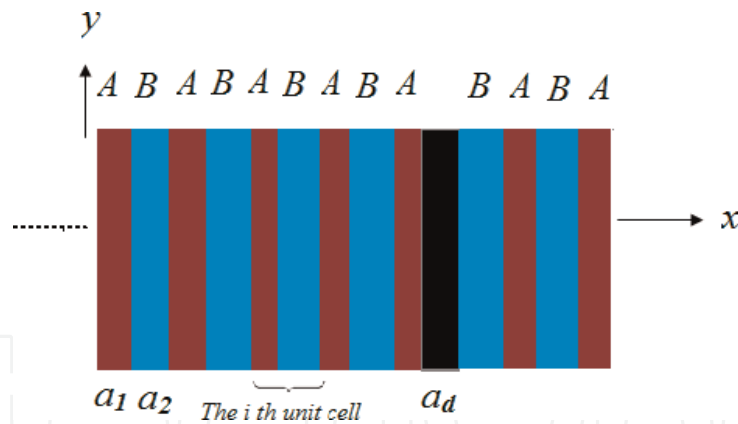


Figure 4.
A schematic diagram of a defect 1D binary PnC.

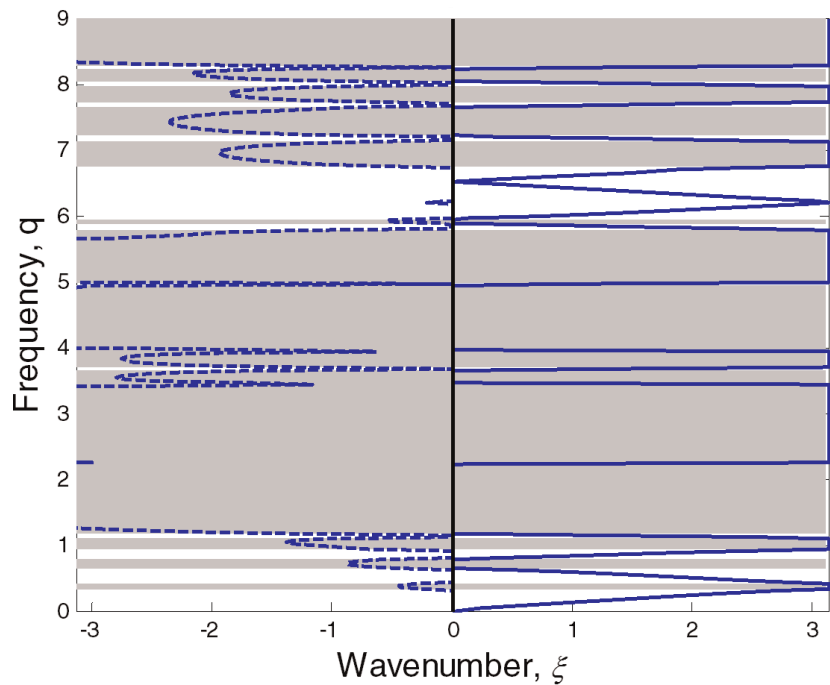


Figure 5.
The dispersion curve of SH-waves propagating in the defected PnC. A defect layer from aluminum with thickness $a_d = a_A$ was immersed between the two periodic unit cells (stop-bands shaded with the gray color).

Not only the thickness of the defect layer has an obvious effect on wave localization but also the type of the defect layer has a significant effect on the localized modes inside the band gaps. Although we introduced two different materials in **Figure 6(c)** and **(d)** with the same thickness, the number and width of the localized peaks had greatly changed. In **Figure 6(c)**, we used Au which has mechanical constants higher than the host materials, while in **Figure 5(d)**, we used nylon which has mechanical constants lower than the host materials. As a result, the width and number of the transmission bands are larger in **Figure 6(d)** than in **Figure 6(c)**. Actually, the nylon is a very soft material like a spring and can introduce more resonant modes inside the PnC structure.

3.1.3 Temperature effects on the band structure of PnC

Now we will investigate the effects of temperature elevation on the PnC structure and phononic band gaps. Two temperature degrees ($T = 35$ and 180°C) were considered. **Figure 7** shows the response of the dispersion relations with

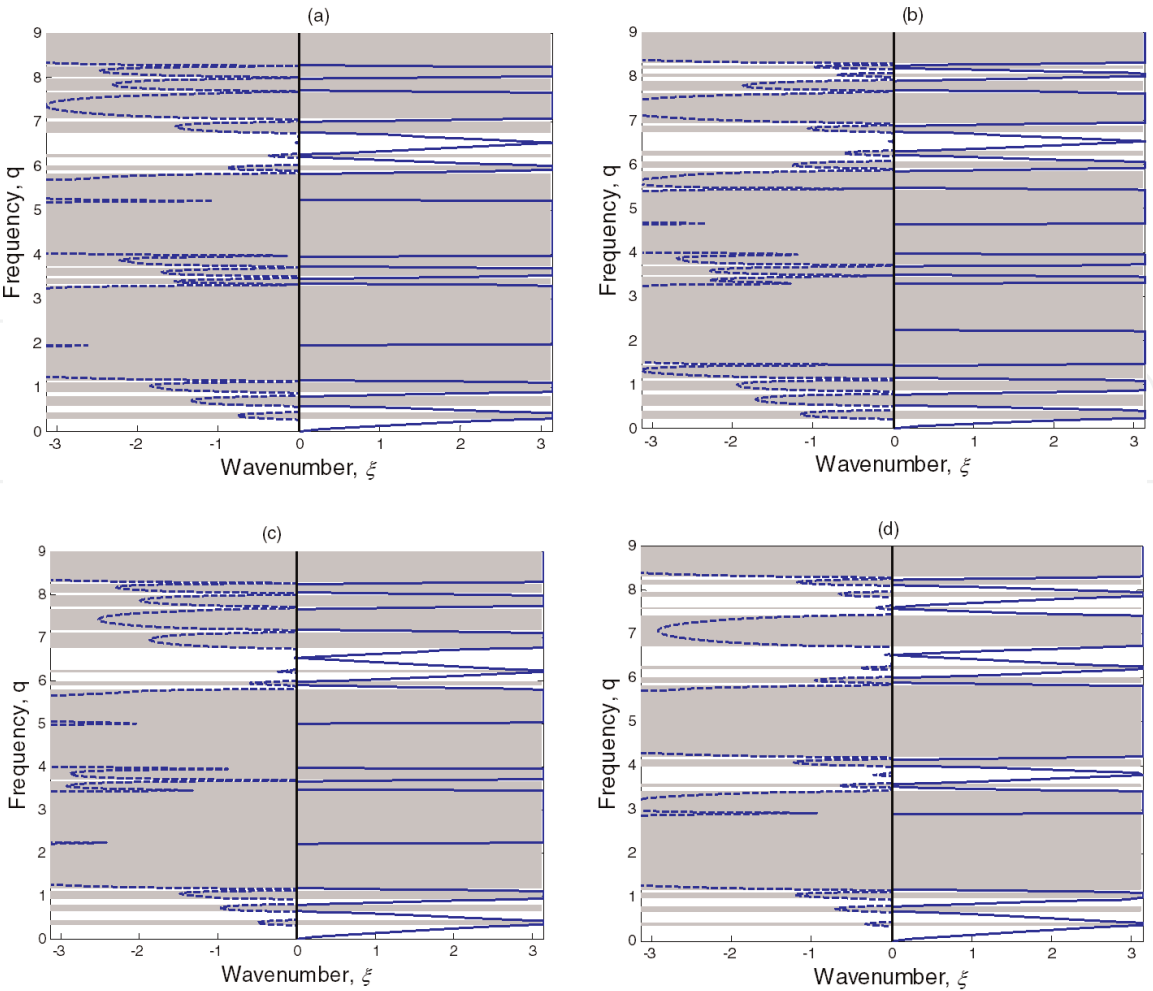


Figure 6. The calculated dispersion curve of SH-waves propagating in a 1D binary defected PnC. (a) $a_d = 2a_A$ (Al), (b) $a_d = 4a_A$ (Al), (c) $a_d = a_A$ (Au), and (d) $a_d = a_A$ (Nylon) (stop-bands shaded with the gray color).

different temperatures at SH-waves propagation through PnCs. We can note in **Figure 7(a)** and **(b)** that, with increasing the temperature from $T = 35$ to $T = 180^{\circ}\text{C}$, respectively, the pass/stop band width remains constant due to the opposite increment in the thermal stress, which has a negative value and maintains materials dimensions constant. Therefore, there is not any variation in the thickness

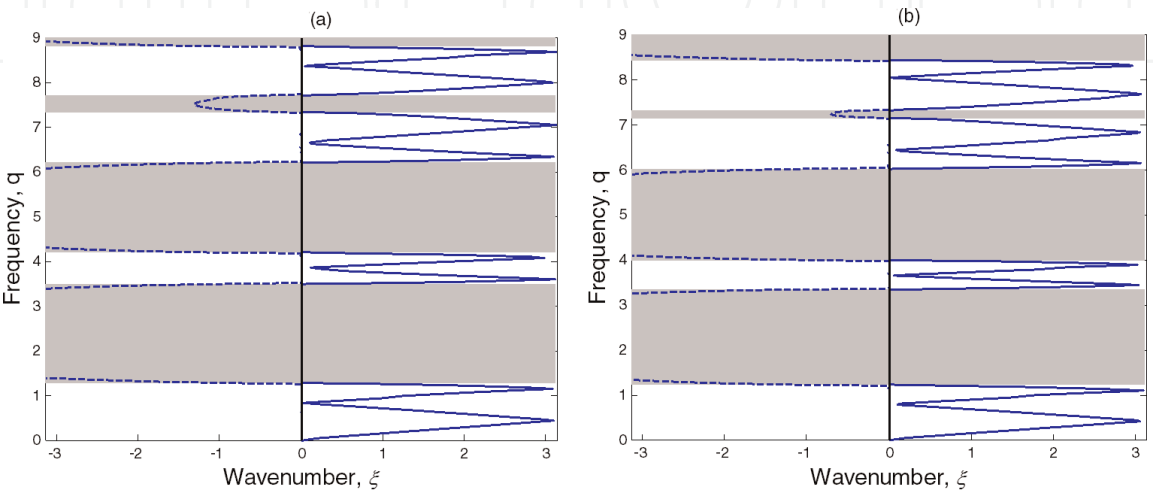


Figure 7. The dispersion curve of SH-waves propagates in a PnC from lead and epoxy materials. Different temperatures are considered. (a) $T = 35^{\circ}\text{C}$ and (b) $T = 180^{\circ}\text{C}$ (stop-bands shaded in gray).

of any material, which in turn keeps the width of the band gaps constant. Finally, we can note only band edges changed slightly with increasing the temperatures. Such small shift in the band gaps is related to the different thermal expansion coefficients of the two materials. Based on this result, the effects of temperature on the PnC structure are greatly related to the type of waves that propagate through crystal structure. Hence, we will verify this result by studying the temperature effects on PnCs at plane wave propagation as well.

3.2 Plane waves results

As depicted in **Figure 1**, we can calculate the reflection coefficient of S- and P-waves in the x -direction through the PnC structure. The PnC structure is proposed to be bonded between two semi-infinite materials (nylon material) at the two ends. The subscripts “0” and “e” denote the left and the right of the PnC structure, respectively.

The reflection coefficient of the displacement field through a PnC structure is given by the form [39],

$$\frac{U_1}{U_0} = \frac{T_{12} + E_0 T_{11} - E_0 E_e T_{21} - E_e T_{22}}{E_0 (T_{11} - E_e T_{21}) - (T_{12} - E_e T_{22})}, \quad (26)$$

where U_1 is the reflected amplitude and $T_{ij} = T(i, j)$ are the elements of the total transfer matrix $T = T_n T_{n-1} \dots T_m \dots T_1$.

Figure 8 shows the relation between the reflectance R versus $\omega a / 2\pi c_T$ (ω is considered the angular frequency in this relation and $c_T = c_{SB}$) for P-wave (red dashed lines) and S-wave (black solid lines) [48]. From **Figure 8**, we can determine the range of frequencies for which the phononic band gaps can be occurred (reflectance of P- and S-waves is high $R \approx 1$). Such high reflectance within the different frequency ranges represents the frequency band gaps of P- and S-waves inside the PnC structure.

From **Figure 8**, it can be seen that the phononic band gaps described by the reflection coefficient are agreed with those described by the dispersion relations.

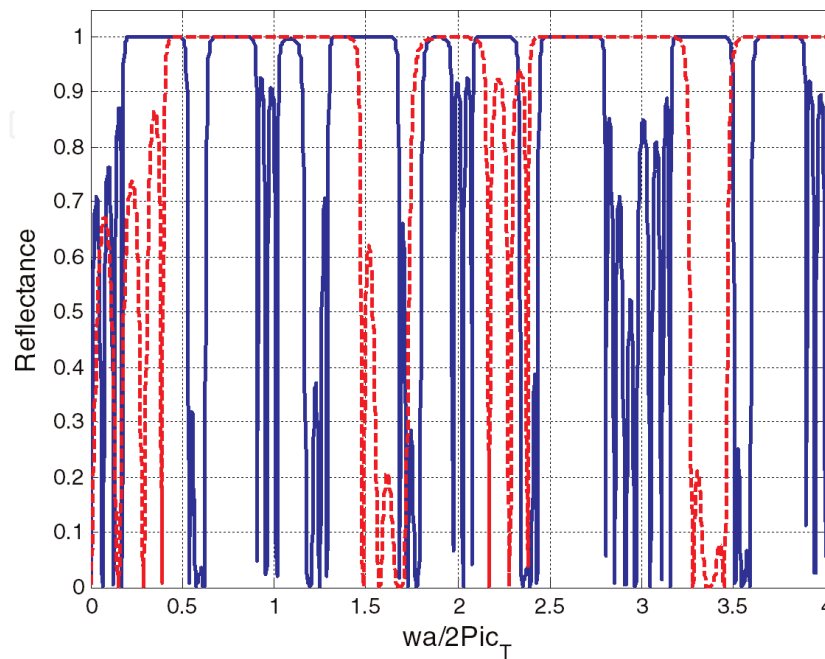


Figure 8.

The reflectance R versus $\omega a / 2\pi c_T$ of P-wave (red lines) and S-waves (blue lines) propagated normally through a 1D PnC structure consist of four unit cells. Each unit cell consists of lead and epoxy materials.

The frequency regions at $R \approx 1$ of P- and S-waves represent the complete band gaps of the plane waves through the PnC structure. There is only a fine difference in the band gaps edges between **Figure 8** and those obtained by the dispersion relation. In **Figure 8**, the relation is plotted between the reflectance and $\omega a/2\pi c_T$, and $c_T = c_{SB}$ is chosen for both P- and S-waves reflectance. Therefore, we will use the reflection coefficient to describe the effects of the defect layer and temperature instead of dispersion relations in order to plot both P- and S-waves in the same graph and for the practical and industrial purpose as well.

3.2.1 Influences of the defect layer/temperature on the phononic band gaps “plane wave”

In this section, we will study the effects of the defect layer and temperatures on the band structure of PnCs at the propagation of plane waves and compare with those investigated for SH-waves.

3.2.1.1 Defect layer influences on band structure

First, we will use the same defected structure used in Section 3.1.2 with the same materials and conditions, only the angle of incidence will be maintained at $\theta_0 = 0^\circ$. **Figure 9** confirms the last results of the effects of the defect layer on the localization modes through the PnC at the plane wave propagation. In **Figure 9(b)**, a number of the localized waves was generated inside the phononic band gaps and was increased by increasing the defect layer thickness as well.

3.2.1.2 Temperature influences on band structure

In this section, the two temperatures $T = 50^\circ\text{C}$ and 190°C were considered in order to illustrate the effects of temperature on the phonic band gaps. We noticed that the phononic band gaps were affected slightly by temperatures at plane wave propagation higher than SH-waves. Therefore, the propagation of elastic waves and localized modes can be affected by temperature elevation. From **Figure 10(a)**, we can note that the reflectance of the P-wave (Red lines) is moved toward the higher frequencies (i.e., band gap at $\omega a/2\pi c_T = 3.5$). Such displacement in the band gap edges is quite noticeable at $T = 190^\circ\text{C}$ in **Figure 10(b)**.

These temperature effects on the band gaps can be explained by two reasons. First, the P-wave velocity is increased according to Eq. (24) because the temperature has a direct effect on the elastic constants. Consequently, temperature makes a

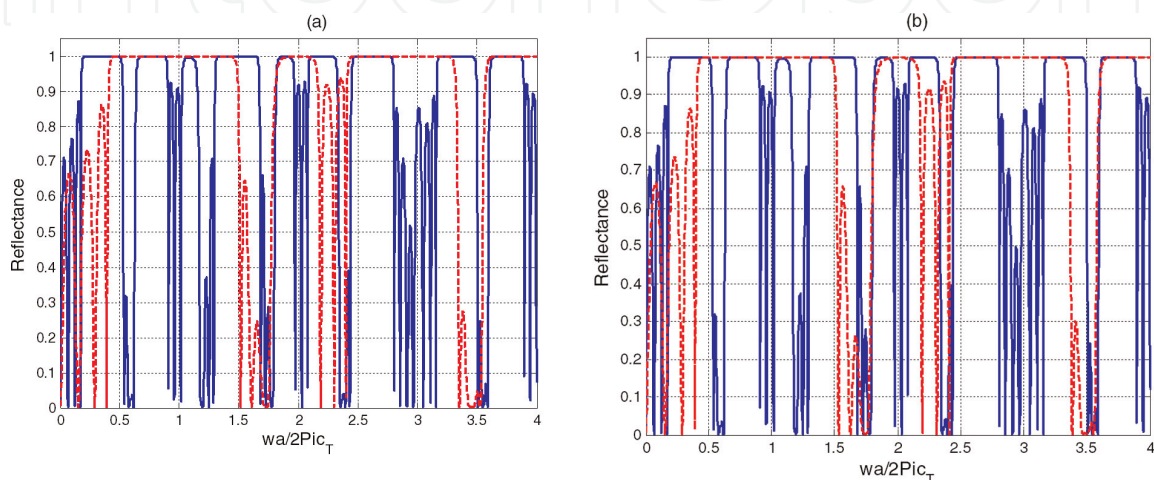


Figure 9.
 (a) Aluminum defect layer with $a_d = a_A$, (b) Aluminum defect layer with $a_d = 4a_A$.

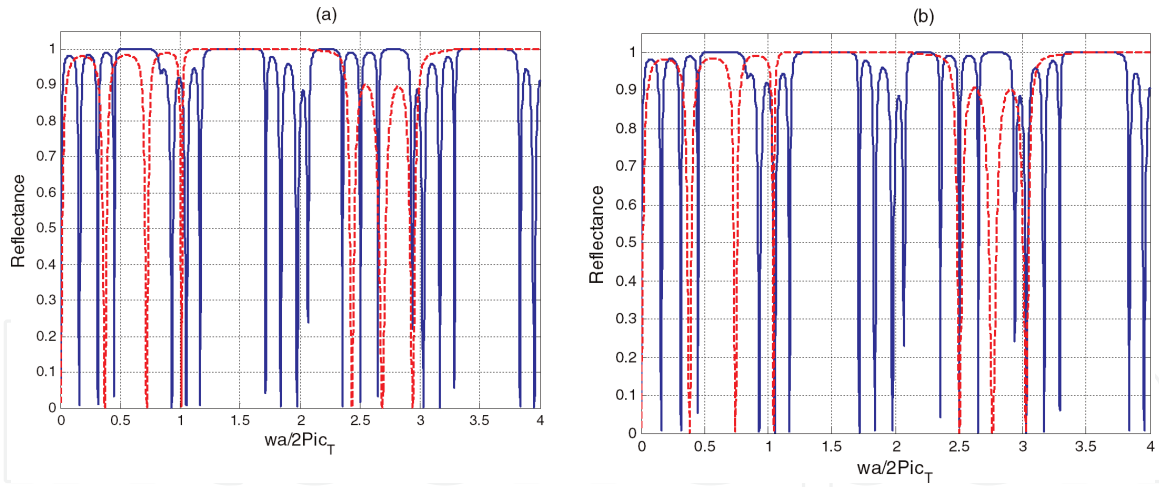


Figure 10. The reflectance R versus $\omega a/2\pi c_T$ for P-wave (red lines) and S-waves (blue lines) at temperatures effects (a) $T = 35^\circ\text{C}$ and (b) $T = 180^\circ\text{C}$.

notable change in the edges of the phononic band gaps. Second, here in the plane wave case, the thermal stress is absent, so the lattice constants will increase according to Eq. (25) and can make change in the width of the phononic band gaps as well.

4. Conclusions

In this chapter, we used the transfer matrix method and Bloch theory to compute and study the propagation of mechanical waves through different 1D PnC structures with thermal effects. We performed numerical simulations to calculate the reflection coefficient and dispersion curves for the 1D PnC structure. We have discussed and studied the effects of many parameters on the phononic band gaps. The effects of temperature and defect mode on the properties of the PnC and on the localized modes were studied for both SH-waves and in-plane waves. The output results can be stated as follows:

1. The defect layer has a different and unique effect on the number of localized modes inside the phononic band gaps for both plane and SH-waves. The effects of the incident angle, thickness ratio on the propagation, and localization of elastic waves were studied. The number of localized modes was increased with increasing the defect layer thickness. Also, the material type of the defect layer has an obvious effect on the width and number of resonant defect modes, where the localized modes were increased by using a material with low elastic constant. Inserting a defect layer inside the perfect structure facilitates the process of localized modes generation inside the PnC structure. Also, it can be utilized in many potential applications such as acoustic filter and waveguides and can be applied to produce new types of laser called phonon laser with low thermal effects especially in the hypersonic PnCs regime.
2. Results revealed that temperature increment has a significant effect on the phononic band gaps and on the number of the localized modes inside the PnC structure, especially for plane wave, where the P-waves velocity and lattice constants are directly related to temperature increment. The contribution of phonons in the thermal conductivity of a solid can be limited by the existence of phononic band gaps, which could be very useful for the thermoelectric

devices that convert thermal energy into electricity. Hence after, the performance of many devices such as Peltier thermoelectric coolers, thermocouples, sensors, and thermoelectric energy generators can be enhanced. Moreover, the thermal conductivity of many structures could experience great changes based on the temperature gradients of PnCs. When temperature is increase in PnCs, the phononic band gap experiences a significant change.

Conflict of interest


The authors declare that there is no conflict of interest.

Author details

Arafa H. Aly* and Ahmed Mehaney
Physics Department, Faculty of Sciences, Beni-Suef University, Egypt

*Address all correspondence to: arafaaly@aucegypt.edu

IntechOpen

© 2019 The Author(s). Licensee IntechOpen. This chapter is distributed under the terms of the Creative Commons Attribution License (<http://creativecommons.org/licenses/by/3.0>), which permits unrestricted use, distribution, and reproduction in any medium, provided the original work is properly cited. 

References

- [1] Gorishyy T, Maldovan M, Ullal C, Thomas E. Sound ideas. *Physics world*. 2005;24-29
- [2] Armenise MN, Campanella CE, Ciminelli C, dell'Olio F, Passaro VMN. Photonic and phononic band gap structures: modeling and applications. *Physics Procedia*. 2010;3:357-364
- [3] Torrent D, Sanchez-Dehesa J. Radial wave crystals: Radially periodic structures from anisotropic metamaterials for engineering acoustic or electromagnetic waves. *Physical Review Letters*. 2009;103:064301
- [4] Fok L, Zhang X. Negative acoustic index metamaterial. *Physical Review B*. 2011;83:214304
- [5] Cai C, Wang Z, Chu Y, Liu G, Xu Z. The phononic band gaps of Bragg scattering and locally resonant pentamode Metamaterials. *Journal of Physics D: Applied Physics*. 2017;50:41
- [6] Warmuth F, Wormser M, Körner C. Single phase 3D phononic band gap material. *Scientific Reports*. 2017;7:3843
- [7] Jia Z, Chen Y, Yang H, Wang L. Designing Phononic Crystals with Wide and Robust Band Gaps. *Physical Review Applied*. 2018;9:044021
- [8] Aly AH, Nagaty A, Khalifa Z. Propagation of acoustic waves in 2D periodic and quasiperiodic phononic crystals. *International Journal of Modern Physics B*. 2017;31
- [9] Christensen J, Fernandez-Dominguez AI, de Leon-Perez F, Martin-Moreno L, Garcia-Vidal FJ. Collimation of sound assisted by acoustic surface waves. *Nature Physics*. 2007;3:851-852
- [10] Aly AH, Mehaney A, Hanafey HS. Phononic band gaps in one dimensional mass spring system. *PIERS Proceeding*. 2012;1047:27-30
- [11] Aly AH, Nagaty A, Khalifa Z, Mehaney A. The significance of temperature dependence on the piezoelectric energy harvesting by using a phononic crystal. *Journal of Applied Physics*. 2018;123:185102
- [12] Aly AH, Mohamed D, Elsayed HA, Mehaney A. Fano resonance by means of the one-dimensional superconductor photonic crystals. *Journal of Superconductivity and Novel Magnetism*. 2018;31:3827-3833
- [13] Aly AH, Mehaney A. Phononic crystals with one-dimensional defect as sensor materials. *Indian Journal of Physics*. 2017;91:1021
- [14] El-Kady I, Olsson RH III, Fleming JG. Phononic band gap crystals for radio frequency communications. *Applied Physics Letters*. 2008;92:233504
- [15] Mehaney A, Eissa MF, Aly AH. Detection and discrimination between alpha particles and protons based on phononic crystals materials. *Surface Review and Letters*. 2018. DOI: 10.1142/S0218625X18502190
- [16] Aly AH, Nagaty A, Mehaney A. One-dimensional phononic crystals that incorporate a defective piezoelectric/piezomagnetic as a new sensor. *The European Physical Journal B*. 2018;91:211. DOI: 10.1140/epjb/e2018-90347-6
- [17] Mohammadi S, Eftekhari AA, Hunt WD, Adibi A. High-Q micromechanical resonators in a two-dimensional phononic crystal slab. *Applied Physics Letters*. 2009;94:051906
- [18] Nagaty A, Mehaney A, Aly AH. Influence of temperature on the

- properties of one-dimensional piezoelectric phononic crystals. Chinese Physics B. 2018;**27**:094301
- [19] Nagaty A, Mehaney A, Aly AH. Acoustic wave sensor based on piezomagnetic phononic crystal. Journal of Superconductivity and Novel Magnetism. 2018;**31**:4173-4177
- [20] Chen JJ, Han X. The propagation of Lamb waves in one-dimensional phononic crystal plates bordered with symmetric uniform layers. Physics Letters A. 2010;**374**:3243-3246
- [21] Chen A, Wang Y, Yu G, Guo Y, Wang Z. Elastic wave localization in two-dimensional phononic crystals with one-dimensional quasi-periodicity and random disorder. Acta Mechanica Solida Sinica. 2008;**21**:517-528
- [22] Torrent D, Sanchez-Dehesa J. Acoustic resonances in two-dimensional radial sonic crystal shells. New Journal of Physics. 2010;**12**:073034
- [23] Liu Z, Zhang X, Mao Y, Zhu YY, Yang Z, Chan CT, et al. Locally resonant sonic materials. Science. 2000;**289**: 1734-1736
- [24] Kushwaha MS, Halevi P, Martinez G, Dobrzynski L, Djafari-Rouhani B. Theory of acoustic band structure of periodic elastic composites. Physical Review B. 1994;**49**:2313-2322
- [25] Tan EL. Generalized eigenproblem of hybrid matrix for Floquet wave propagation in one-dimensional phononic crystals with solids and fluids. Ultrasonics. 2010;**50**:91-98
- [26] Pennec Y, Djafari-Rouhani B, Vasseur JO, Khelif A, Deymier PA. Tunable filtering and demultiplexing in phononic crystals with hollow cylinders. Physical Review E. 2004;**69**: 046608
- [27] Lucklum R, Li J, Zubtsov M. 1D and 2D phononic crystal sensors. Procedia Engineering. 2010;**5**:436-439
- [28] Zhao D, Wang W, Liu Z, Shi J, Wen W. Peculiar transmission property of acoustic waves in a one-dimensional layered phononic crystal. Physica B. 2007;**390**:159-166
- [29] Zhang X, Liu YY, Wu FG, Liu ZY. Large two-dimensional band gaps in three-component phononic crystals. Physics Letters A. 2003;**317**:144-149
- [30] Ciminelli C, Peluso F, Armenise MN. Modelling and design of two-dimensional guided-wave photonic band-gap devices. IEEE Journal of Light wave Technology. 2005;**23**:886-901
- [31] Taflov A. Computational Electrodynamics: The Finite-Difference Time -Domain method. Norwood, MA: Artech House Inc; 1995
- [32] Dwoyer DL, Hussaini MY, Voigt RG. Finite Element-Theory and Application. New York: Springer-Verlag; 1986
- [33] Zhao HG, Liu YZ, Wen JH, Yu DL, Wen XS. Tri-component phononic crystals for underwater anechoic coatings. Physics Letters A. 2007;**367**: 224-232
- [34] Thomson WT. Transmission of elastic waves through a stratified solid medium. Journal of Applied Physics. 1950;**21**:89-93
- [35] Liu L, Hussein MI. Wave motion in periodic flexural beams and characterization of the transition between Bragg scattering and local resonance. Journal of Applied Mechanics. 2012;**79**:011003
- [36] Hussein MI, Hamza K, Hulbert GM, Scott RA, Saitou K. Multiobjective evolutionary optimization of periodic layered materials for desired wave

- dispersion characteristics. *Structural Multidisciplinary Optimization*. 2006; **31**:60-75
- [37] Aly AH, Mehaney A. Modulation of the band gaps of phononic crystals with thermal effects. *International Journal of Thermophysics*. 2015;**36**:2967
- [38] Ciampa F, Mankar A, Marini A. Phononic crystal waveguide transducers for nonlinear elastic wave sensing. *Scientific Reports*. 2017;**7**:14712
- [39] Wu LY, Yang WP, Chen LW. The thermal effects on the negative refraction of sonic crystals. *Physics Letters A*. 2008;**372**:2701-2705
- [40] Hopkins PE, Phinney LM, Rakich PT, Olsson III RH, EL-Kady I. Phonon considerations in the reduction of thermal conductivity in phononic crystals. In: *MeTA'10 2nd International Conference on Metamaterials, Photonic Crystals and Plasmonics*. 2010. pp. 308-316
- [41] Aly AH, Mehaney A, El-Naggar SA. Evolution of phononic band gaps in one-dimensional phononic crystals that incorporate high-T_c superconductor and magnetostrictive materials. *Journal of Superconductivity and Novel Magnetism*. 2017;**30**:2711-2716
- [42] Chen AL, Wang Y-S. Study on band gaps of elastic waves propagating in one-dimensional disordered phononic crystals. *Physica B*. 2007;**392**:369-378
- [43] Aly AH, Mehaney A. Low band gap frequencies and multiplexing properties in 1D and 2D mass spring structures. *Chinese Physics B*. 2016;**25**:114301
- [44] Aly AH, Mehaney A, Eissa MF. Ionizing particle detection based on phononic crystals. *Journal of Applied Physics*. 2015;**118**:064502
- [45] Rose JL. *Ultrasonic Waves in Solid Media*. London: Cambridge University Press; 1999
- [46] Wang YZ, Li FM, Kishimoto K, Wang YH, Huang WH. Wave localization in randomly disordered layered three-component phononic crystals with thermal effects. *Archive of Applied Mechanics*. 2010;**80**:629-640
- [47] Shang FL, Wang ZK, Li ZH. An exact analysis of thermal buckling of piezoelectric laminated plates. *Acta Mechanica Solida Sinica*. 1997;**10**:95-107
- [48] Li FM, Wang YS. Study on wave localization in disordered periodic layered piezoelectric composite structures. *International Journal of Solids Structures*. 2005;**42**:6457-6474
- [49] Hussein MI, Hulbert GM, Scott RA. Dispersive elastodynamics of 1D banded materials and structures: analysis. *Journal of Sound and Vibration*. 2006; **289**:779-806
- [50] Aly AH, Mehaney A. Enhancement of phononic band gaps in ternary/binary structure. *Physica B: Condensed Matter*. 2012;**407**(21):4262-4268
- [51] Gray DE, Fischel DN, Crawford HB, Douglas DA, Eisler WC. *American Institute of Physics Handbook*. 3rd ed. USA: Colonial Press, McGraw-Hill Book Company; 1972
- [52] Mason WP. *Piezoelectric Crystals and Their Application to Ultrasonics*. Princeton, N. J: D. Van Nostrand Company, Inc; 1950. pp. 480-481
- [53] Serway RA, Jewett JW. *Physics for Scientists and Engineers*. 6th ed. USA: Thomson Brooks/Cole; 2004
- [54] Aly AH, Mehaney A, Rahman EA. Study of physical parameters on the properties of phononic band gaps. *International Journal of Modern Physics B*. 2013;**27**:1350047
- [55] Mehaney A. Phononic crystal as a neutron detector. *Ultrasonics*. 2019;**93**: 37-42